Mechanical characterization of anisotropic elasto-plastic materials by indentation curves only

V. Buljak · M. Bocciarelli · G. Maier

Abstract Anisotropy, usually orthotropy, arises in structural materials, particularly metals, due to production processes like laminations and concerns primarily parameters which govern the plastic behavior. Identification of such parameters is investigated here by a novel approach with the following features: experimental data provided by indentation curves only (not by imprint geometry); indenter shape with elliptical cross-section derived from classical conical or spherical shape and optimized by sensitivity analyses; indentation test repeated in near places after indenter rotation; deterministic inverse analyses centered on discrepancy function minimization and made computationally economical by an 'a priori' model reduction procedure.

Keywords Anisotropy · Elastoplasticity · Indentation · Inverse analysis

This paper is dedicated to Professor Piotr Perzyna, outstanding scientist in solid mechanics, who passed away last year.

V. Buljak
Department of Strength of Materials, University of Belgrade Faculty of Mechanical Engineering, Kraljice Marije 16, Belgrade, Serbia

M. Bocciarelli (✉)
Architecture, Built Environment and Construction Engineering Department, Politecnico di Milano (Technical University), piazza Leonardo da Vinci 32, 20133 Milan, Italy
e-mail: massimiliano.bocciarelli@polimi.it

G. Maier
Department of Structural Engineering, Politecnico di Milano (Technical University), piazza Leonardo da Vinci 32, 20133 Milan, Italy
e-mail: giulio.maier@polimi.it

1 Introduction

Estimation of parameters in material models is often necessary for diagnostic analyses of possibly deteriorated existing structures and plant components and for controls of industrial production processes and their products. Since many years indentation tests have been used as practical, mostly nondestructive methodology for material characterization. Not only hardness, like in the remote origin of this experimental methodology (see e.g. [1, 2]), but also material properties such as Young's modulus and yield stress can be inferred from the indentation tests. The transition from hardness tests to indentation tests, intended to assess mechanical properties of structural materials, has been promoted by the possibility of performing such experiments economically on site, by their "quasi-non-destructiveness" (i.e. without extracting specimens for laboratories) and by the growing need to accurately identify parameters involved in modern structural analyses procedures. Clearly "non-destructive" are resonance tests which are at present employed for mechanical characterizations of anisotropic materials but they exhibit obvious limitations to linear elasticity.

Anisotropy of elastic and plastic properties are often exhibited by rolling sheets, composites and coatings. In order to determine the mechanical properties of these materials, still tensile and compressive tests are usually performed along different directions. Such invasive and "destructive" procedure might be advantageously replaced by the indentation based method proposed herein, apt to test the material locally without extracting specimens and without measuring imprint geometry.

The recently proposed parameter identification methodologies based on indentation experiments include the following developments, accompanied by improvements and innovations in experimental equipments (details, e.g. in references [3–8]): (i) inverse analysis methods, namely mathematical and numerical techniques for the transition from quantities measurable in the test to the sought parameters; (ii) measurements concerning the imprint geometry (e.g.: by laser profilometers at macro-scale, by atomic force microscope at the nano-scale), besides or instead of, the loading versus penetration relationship ("indentation curves") provided by the "instrumented" indenter.

The latter development, i.e. recourse to experimental data on imprint, was proposed in order to enrich the input for inverse analyses, [3], and has been investigated to various purposes, including calibration of anisotropic models, [4]. In fact tensorial entities, such as residual stresses or material anisotropy models, cannot be "calibrated" through parameter estimation based on a single indentation test by a traditional indenters with axially symmetric tip (Brinell, Rockwell, Vickers, etc.): the resulting indentation curves (on loading and unloading phases of the test) obviously reflect only direction-insensitive, average, features of the investigated system.

Indentation of anisotropic solids has been the subject of research carried out from both theoretical and applicative point of views; see, e.g.: [5–8]. Methods based on indentation to estimate elastic properties of anisotropic materials have been developed particularly in the biomechanical field, see e.g. [9, 10]. These techniques rest on correlation formulae of the sought parameters with the "indentation modulus" (i.e., the initial slope of the indentation curve during unloading), which can be evaluated as weighted average of the elastic constants as shown in [5, 7, 8].

Calibration of anisotropic elastic–plastic material models still represents a practically meaningful challenge which arises in diverse technological areas. Although indentation-based methods to identify elastic–plastic material properties for isotropic materials are well established, methods for anisotropic materials are still a timely research subject. In [11, 12] a method based on dimensionless functions and on information consisting of indentation curve and on some geometrical features of the imprint is proposed for the identification of three parameters: two yield stresses and a hardening coefficient. The same experimental information had been used in [4] to identify by means of inverse analysis, seven parameters: three elastic moduli, three plastic parameters and the friction coefficient between indenter and specimen surface. In [13] a Kalman filter based approach is adopted in order to estimate five parameters (two elastic moduli, two yield stresses and one hardening coefficient) using information collected from a dual indentation method.

The employment of laser profilometers on site (or in laboratory after transferring to it imprint shapes by suitable casts) provides experimental data additional to indentation curves in order to estimate tensorial quantities [14], but obviously implies additional costs and time. For assessment of residual stress tensor components a new indentation procedure based on instrumented indenter only, with novel optimized elliptical cross-section was recently proposed and investigated in [15]. The results achieved in [14, 15] and validated by numerical exercises concern the three stress components which govern a plane stress state near the surface of a weld or of a structural component produced by metal forming.

The present study aims at the development of a procedure for mechanical characterization of anisotropic materials by means of indentation curves alone.

The parameter identification procedure studied herein is characterized by the following peculiar methodological features: (i) novel indenter shape derived from either conical or spherical original geometries, with elliptical cross-section governed by parameters to be optimized by sensitivity analyses; (ii) experimental data acquired from indentation curves only, generated by two tests, in near sites, with the ellipse principal axis rotated by 90°; (iii) inverse analysis based on such experimental data and carried out economically by mathematical programming minimization of the "discrepancy function"; (iv) the minimization algorithm made much faster by means of an "ad hoc" software, generated once for all, on the

basis of "a priori" performed finite element simulations of the tests and "compressed" by a "proper orthogonal decomposition" (POD) procedure for "model reduction".

Since "elliptical" indenters, upon whom the proposed procedure is based, are not yet available in the market, truly experimental data could not be used to validate the novel method. Therefore "pseudo-experimental" data were used, i.e. data which are generated through the same finite element model adopted to simulate the indentation test, by assigning certain values to the sought parameters, values which then are compared to those found as output of the inverse analysis procedure.

The paper is organized as follows. Sect. 2 describes the adopted material model with some "ad hoc" conjectures on lower and upper bounds of each parameter to estimate. The anisotropic model considered in this paper is Hill's constitutive law for associative, "perfect" (i.e. ductility with negligible hardening) elasto-plasticity, see e.g. [16–18]. The proposed new geometry of indenter and test simulations by a finite element (FE) commercial code, [19], accounting for large-strain regime, are preliminarily presented in Sect. 3. Sensitivity analyses apt to quantify the influence of the sought parameters on measurable data are employed in Sect. 4, primarily for the design of novel indenters by optimization of the parameters governing their shapes. Section 5 is devoted to applications of the above mentioned POD preliminary procedure associated to "trust region algorithm" (TRA), with reference, for details, to available literature, e.g. [20]. Section 6 presents parameter estimation exercises based on a constrained optimization technique with attention paid to possible non-convexity of the discrepancy function to minimize and to relevant literature as e.g. [21–24]. Conclusions and prospects of further research on this and related items are outlined in Sect. 7.

2 Anisotropic material modeling with parameters to estimate

The material model adopted in the present study is the classical associative elastic-perfectly-plastic constitutive model proposed by Hill (1948) [16], which can be expressed by the following relationships, e.g. [17]:

$$\dot{\varepsilon}_{ij} = \dot{\varepsilon}^{el}_{ij} + \dot{\varepsilon}^{pl}_{ij}, \quad \dot{\sigma}_{ij} = D_{ijkl}\dot{\varepsilon}^{el}_{kl}, \quad \dot{\varepsilon}^{pl}_{ij} = \dot{\lambda}\frac{\partial f}{\partial \sigma_{ij}} \quad ((1))$$

$$f\left(\sigma_{ij}\right) = k_{11}(\sigma_{22}-\sigma_{33})^2 + k_{22}(\sigma_{11}-\sigma_{33})^2 + k_{33}(\sigma_{22}-\sigma_{11})^2 + k_{23}\sigma_{23}^2 + k_{13}\sigma_{13}^2 + k_{12}\sigma_{12}^2 - 1 \quad (2)$$

$$f \le 0; \quad \dot{\lambda} \ge 0; \quad f\dot{\lambda} = 0 \quad (3)$$

In the above equations ε_{ij} represents the strain tensor decomposed into the elastic ε^{el}_{ij} and plastic ε^{pl}_{ij} components; D_{ijkl} is the fourth-order anisotropic elasticity tensor; $f(\sigma_{ij})$ is the yield function which defines the elastic domain (constant here in the absence of hardening) and the direction of the plastic strains according to an associative flow rule and λ represents the plastic multiplier.

Linear elasticity in an orthotropic material is characterized by the following engineering constants, which define the elastic tensor components D_{ijkl}: principal direction elastic moduli E_1, E_2, E_3, Poisson's ratios ν_{12}, ν_{23}, ν_{13}, and shear moduli G_{12}, G_{23}, G_{31}.

The yield criterion proposed by Hill is a straightforward generalization to anisotropy of Huber–Mises criterion. The six material parameters k_{ij} in Eq. (2) are related to the yield stresses (σ^Y_{11}, σ^Y_{22}, σ^Y_{33}, same in tension and compression) along the three orthotropy axes and to the three shear yield stresses in the three planes of symmetry (τ^Y_{12}, τ^Y_{23}, τ^Y_{13}), according to the following relationships:

$$\begin{aligned} k_{11} &= \frac{1}{2}\left(\frac{1}{\sigma^{Y2}_{22}} + \frac{1}{\sigma^{Y2}_{33}} - \frac{1}{\sigma^{Y2}_{11}}\right), \\ k_{22} &= \frac{1}{2}\left(\frac{1}{\sigma^{Y2}_{11}} + \frac{1}{\sigma^{Y2}_{33}} - \frac{1}{\sigma^{Y2}_{22}}\right), \\ k_{33} &= \frac{1}{2}\left(\frac{1}{\sigma^{Y2}_{11}} + \frac{1}{\sigma^{Y2}_{22}} - \frac{1}{\sigma^{Y2}_{33}}\right) \end{aligned} \quad (4a)$$

$$k_{12} = \frac{1}{\tau^{Y2}_{12}} \quad k_{23} = \frac{1}{\tau^{Y2}_{23}} \quad k_{13} = \frac{1}{\tau^{Y2}_{13}} \quad (4b)$$

The numerical tests for the preliminary validation of the proposed method will be restricted to orthotropic materials with transversal isotropy, the isotropy plane being orthogonal to x_1 axis. Such restriction turns out to be frequently acceptable in engineering practice concerning laminated products. Consequently, the independent plasticity parameters are defined by the following relationships:

$$\sigma_{22}^Y = \sigma_{33}^Y \equiv \sigma_t^Y, \quad \sigma_{11}^Y \equiv \sigma^Y, \\ \tau_{12}^Y = \tau_{23}^Y = \tau_{13}^Y \equiv \sigma_t^Y \Big/ \sqrt{3} \tag{5}$$

The last equation is a reasonable assumption which reduces the number of parameters to be identified, see e.g. [4].

Five independent parameters characterize the elastic response of a transversally isotropic material, namely:

$$E_2 = E_3 \equiv E_t, \quad E_1 \equiv E \tag{6a}$$

$$\nu_{12} = \nu_{13} \equiv \nu, \quad \nu_{23} \equiv \nu_t, \quad G_{12} = G_{13} \equiv G, \\ G_{23} = E_t/2(1+\nu_t) \tag{6b}$$

Assuming that the Poisson's ratios are a priori known and that the coefficient G can be estimated according to $G = E/2(1+\nu)$, the whole set of parameters to be identified consists of the elastic moduli E and E_t and the yield stresses σ^Y and σ_t^Y .

The classical assumption of "perfect plasticity" and unbounded ductility are adopted here in view of two circumstances, namely: such assumptions are acceptable in present engineering practice for ductile metals in many structural components; simplifications of material models are suitable in the present preliminary study of potentialities and limitations of a novel method in inverse analyses. Such limitations will be tackled and partly removed in future developments with consideration of hardening, softening and limited ductility.

3 Preliminary design of the experiment by its simulation

The indentation test to be performed within the present study must provide experimental data in the form of indentation curves, to be used as inputs in the inverse analysis procedure, namely digitalized pairs of preselected loading force and corresponding penetration of the indenter tip into the specimen. In order to strengthen sensitivity of the indentation curves with respect to the parameters of an anisotropic material, a novel shape is attributed to the indenter tip, namely the indenter cross-section orthogonal to its axis is assumed to be an ellipse with ratio r between maximum D and minimum d (principal) diameters.

Within this preliminary study, two alternative kinds of indenter shapes are considered: (A) one generated starting from an original conical Rockwell shape (see Fig. 1a) and (B) the other starting from an original spherical shape (see Fig. 1b). Denoting with $D_0(x)$ the diameter of the original circular cross-section at arbitrary coordinate x measured along the perpendicular axis, the new shape of the elliptical cross-section in both cases is defined by the following relationships:

$$D = \alpha D_0(x), \quad d = \frac{1}{\alpha} D_0(x), \quad r = \frac{D(x)}{d(x)} = \alpha^2 \tag{7}$$

where coefficient α controls the "ellipticity" of the resulting indenter shapes. Clearly, a second parameter governs the geometry of the new diameters, namely: (A) as for the indenter generated from a cone, and here called henceforth "elliptical", this parameter is the opening angle β of the original cone (Fig. 1a); (B) for the sphere-generated indenter (denominated "ellipsoidal" henceforth) the radius R of the original sphere (Fig. 1b).

In the computational examples presented in what follows, to the coefficient α is attributed value 1.4, while to the other two parameters the following values are assumed: $\beta = 60°$ and R = 0.4 mm. The consequent indenter shapes are visualized in Fig. 2a, b for "elliptical" and "ellipsoidal" indenters, starting from conical and spherical shapes respectively.

For the computational exercises to be presented in the sequel of this paper, the following features are assumed for the indenter material: diamond, isotropic linear elasticity with Young's modulus E = 1100 GPa and Poisson's ratio v = 0.1. The structural material to be characterized in preliminary investigations of this novel procedure is aluminum, made anisotropic by some production process like lamination.

To the specimen, orthotropic behavior is attributed with isotropy according to Eqs. (5) and (6) in the "transversal plane" (axes 2 and 3 in the reference system employed in Sect. 2) orthogonal to the lamination direction (axis 1) and to the surface of the structure or specimen to be indented. The following elastic–plastic parameters are assumed: $E = 70$GPa, $E_t = 50$GPa, $\nu = 0.3$, $\nu_t = 0.3$, $G = 27$ GPa, $\sigma_t^Y = 70$ MPa, $\sigma^Y = 100$ MPa. These values can be regarded as typical and representative for orthotropic aluminum sheets.

The maximum load applied on the indenter within the indentation test is assumed equal to 200 N. The penetration, namely imprint depth, is expected to reach values between 0.1 and 0.3 mm, depending on the geometry of the indenter used.

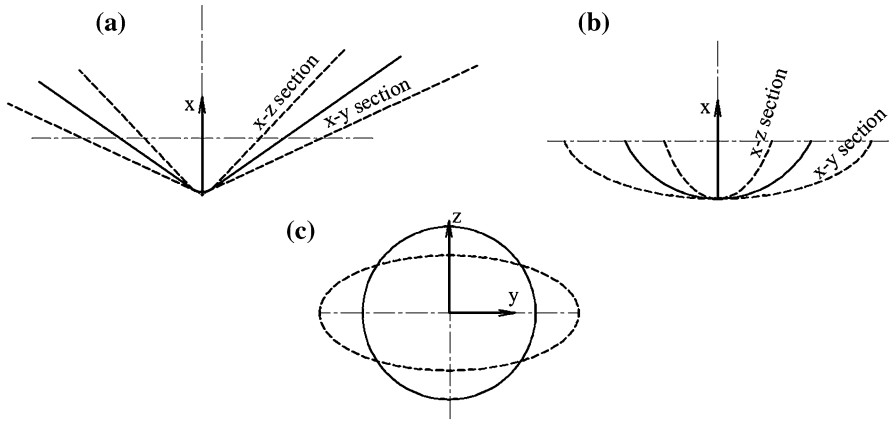

Fig. 1 New indenter shapes starting from: **a** conical indenter; **b** spherical indenter; **c** elliptical cross-section, same for both shapes

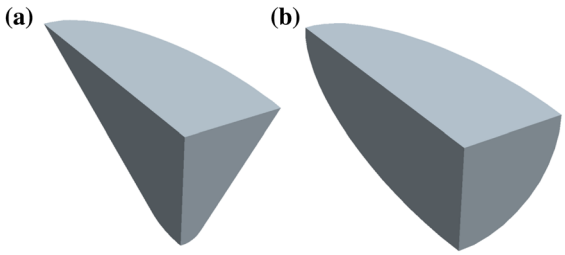

Fig. 2 Shapes of two novel indenters with $\alpha = 1.4$: **a** "elliptical" constructed starting from a conical indenter with angular amplitude $\beta = 60^0$; **b** "ellipsoidal" generated from a spherical indenter with R = 0.4 mm

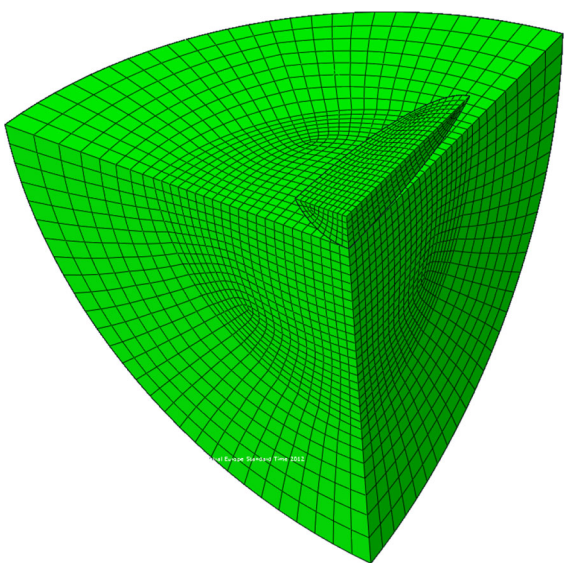

Fig. 3 A typical finite element mesh for test simulations (double symmetry exploited only when principal directions are known)

The finite element (FE) test simulations are carried out by the commercial code Abaqus 6.10.1, [19], with consideration of the indenter as linear elastic. The discretization mesh consists of 8-node hexahedron elements, with a total amount of about 32000 DOF. Figure 3 shows the adopted mesh for an indentation test by an ellipsoidal (originally spherical) indenter. Similar is the mesh considered for tests by elliptical indenter.

The domain considered for the FE simulations and visualized in Fig. 3 is such that on its boundary connecting it to the surrounding material zero displacements may be imposed as boundary conditions of reasonable approximation. The whole domain will be considered in the FE analyses, unless double symmetry can be exploited, i.e. when principal directions are a priori known.

It is worth noting that FE simulations will be performed here in a "large-strain" regime as obviously required by responses to indentations. However, consequences on modeling are not discussed here, as they are general computational features dealt with in the literature and implemented in the adopted commercial code Abaqus, [19]. Critical assessments of modeling and implementation in the above code can be omitted herein because the data for inverse analyses are "pseudo-experimental", namely computed by the same test simulations (same code) employed for inverse analyses, with comparable possible inaccuracy.

4 Indenter shape optimization by sensitivity analysis

Preliminary optimization of the indenter shape by means of comparative numerical exercises is presented in this Section, in order to evidence the possibility to

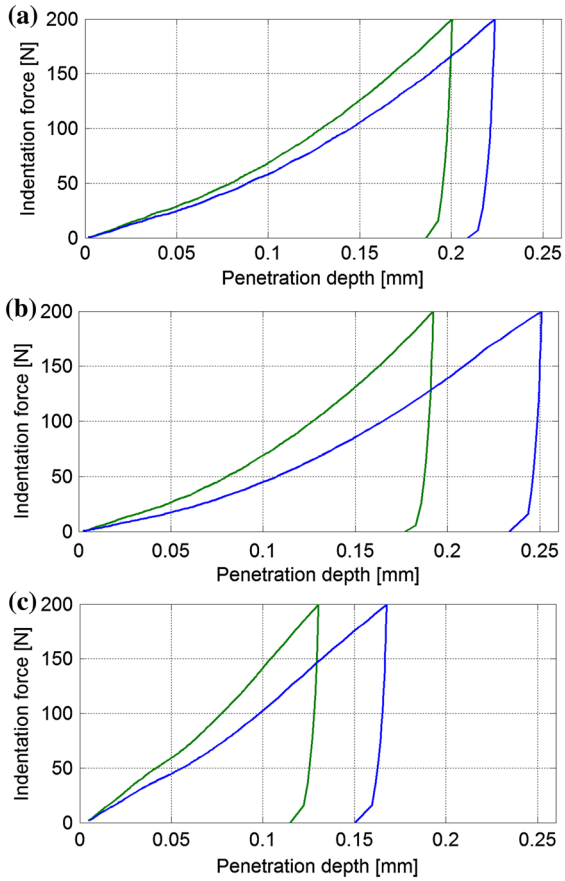

Fig. 4 Couples of indentation curves resulting from the double indentations performed by three different "elliptical" indenters: **a** with $\alpha = 1.2$; **b** with $\alpha = 1.4$; **c** with $\alpha = 2.0$

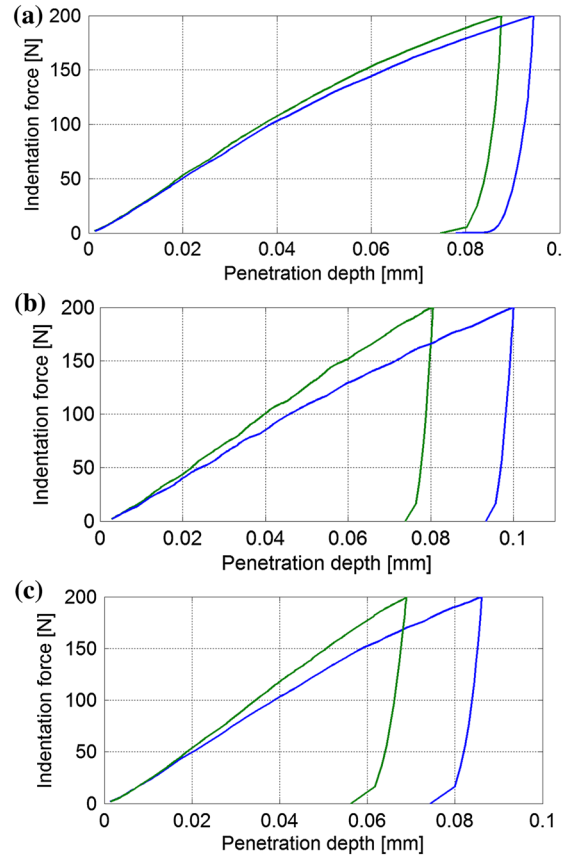

Fig. 5 Couples of indentation curves resulting from the double indentations performed by three ellipsoidal indenters: **a** with $\alpha = 1.2$; **b** with $\alpha = 1.4$; **c** with $\alpha = 2.0$

assess anisotropic properties using data collected from indentation curves only. An orthotropic material model is considered for the specimen with transversal isotropy, with assumptions and reference values of parameters specified in Sect. 3. Two indentation tests are simulated with the principal directions of indenter cross-section coinciding with the orthotropic directions, therefore rotated by 90° from the first test to the second test. If the two resulting indentation curves turn out to be more separated from each other, the indenter shape is preferable, since larger is the direction-dependence of the experimental data from the sought parameters (i.e. of orthotropic material parameters). This criterion is adopted herein for a preliminary selection of the indenter shape. Later sensitivity analysis will be performed in a traditional sense, namely by computing the derivatives of measurable quantities with respect to sought parameters, see e.g. [25].

Figures 4 and 5 summarize results obtained with six different geometries of tested indenters. The first three are of the "elliptical" type visualized in Fig. 2a, starting from a classical conical shape (like Rockwell indenter). Three different values are attributed to the parameters governing the resulting "ellipticity" (see Fig. 1 and Eq. 7), specifically $\alpha = 1.2$, $\alpha = 1.4$ and $\alpha = 2$. The same value is assumed in all three indenters for the opening angle β of the original cone, namely $\beta = 60°$, like for the most popular Rockwell cone.

In the second set of exercises presented herein three indenters have as original geometry a spherical indenter with radius equal to 0.4 mm (Fig. 2b). Relatively small value of original sphere radius is attributed to this indenter in order to keep comparable penetration depths of two types of indenters: "elliptical" (starting from cone) and "ellipsoidal" (starting

from sphere), with the same value of indentation force. To the "ellipsoidal" indenter, the same values are assumed for parameter α, which governs ellipticity according to Eq. (7), namely: $\alpha = 1.2$, $\alpha = 1.4$ and $\alpha = 2$.

Numerical exercises like those with some results visualized in Figs. 4 and 5, have led to the following conclusions: (i) relatively large (and hence accurately measurable) turn out to be in all six test simulations the abscissa differences between the two indentation curves generated by the two tests with maximum diameter of the indenter-cross section parallel to the principal directions of orthotropic material model; (ii) such difference, first increases when ellipticity factor α changes from 1.2 to 1.4, and then slightly decreases for further enlargement of α, up to the value of 2.0; (iii) at equal loading force, growing ellipticity ratio α reduces the penetration depth (hence the test "damage" decreases) and increases in percentage (and slightly decreases in absolute value) the difference of maximum depths between the two tests.

It is worth noting that the imprint, which is caused by indentation intended to calibrate mechanical model of a material as a continuum, should be by at least one or two orders of magnitude larger than representative lengths of the material microstructure and of surface roughness after cleaning. Such requirement turns out to be satisfied by all six examples of Figs. 4 and 5, under the common maximum force of 200 N.

The above remarks, founded on a limited set of merely orientative numerical simulations, lead to the following choice as indenter shape for the subsequent study: originally conical with angle $\alpha = 60^0$, transformed into elliptical indenter with ellipticity parameter $\alpha = 1.4$.

Now, with reference to the above selected elliptical indenter and to the double indentation tests (performed twice in the orthotropic principal directions on the specimen surface), the following usual sensitivity analysis represents a useful check of the proposed procedure. The reference values specified in Sect. 3 are attributed to all material parameters and are indicated by overlined symbols ($\bar{E}, \bar{E}_t, \bar{\sigma}^Y, \bar{\sigma}_t^Y$). Each one of the four parameters to identify (namely E, E_t, σ^Y and σ_t^Y represented in Table 1 by the common symbol X) are incremented in turn of a small percentage, here 5 %, of its reference value. Before and after such increment the maximal penetration depths, say d_I and d_{II}, of the two indentations are computed by FE test simulations. By such numerical results the derivatives of the two measurable quantities d_I and d_{II} with respect to the sought parameters are approximated by forward finite differences. These finite differences after adimensionalization by reference values ($\bar{X}$ and consequent $\bar{d}_I$ and $\bar{d}_{II}$) are gathered in Table 1 and quantify the sensitivities as influence of parameters to estimate on measurable quantities.

Table 1 Adimensionalized sensitivities of the two measurable indentation depths d_I and d_{II} with respect to the parameters to estimate (X)

	E	E_t	σ^Y	σ_t^Y
$\frac{\Delta d_I}{\Delta X} \cdot \frac{\bar{X}}{\bar{d}_I}$	0.067	0.079	0.124	0.132
$\frac{\Delta d_{II}}{\Delta X} \cdot \frac{\bar{X}}{\bar{d}_{II}}$	0.030	0.119	0.128	0.127

The above results of computations according to the traditional sensitivity concepts, see e.g. [25, 26], show that the identification of the four parameters considered herein is quite possible by the proposed double indentation procedure. Clearly, the above evidenced influence of the four parameters on some dominant measurable quantity is transferable to a norm concerning all the experimental data to be dealt with for the inverse analyses presented in the subsequent Section.

5 Inverse analysis

5.1 Discrepancy minimization by mathematical programming

On the basis of experimental data, parameters enclosed in the computational model of the system can be estimated by diverse approaches, either deterministic or stochastic, see e.g. [26, 27].

Here the simplest, most popular, deterministic approach is adopted, namely: the estimates to compute ($\bar{E}, \bar{E}_t, \bar{\sigma}^Y, \bar{\sigma}_t^Y$, included in vector $\hat{\mathbf{p}}$) are the parameter values which minimize a suitable "discrepancy function" ω, specifically:

$$\omega(\hat{\mathbf{p}}) = \min_{p}\{\omega(\mathbf{p})\},\ \omega(\mathbf{p}) = \|\mathbf{u}(\mathbf{p}) - \bar{\mathbf{u}}\| \tag{8}$$

Here vector $\bar{\mathbf{u}}$ gathers the N experimental data (or "pseudoexperimental"), while vector $\mathbf{u}$ contains their

counterparts computed by test simulations as functions of the variable parameter vector $\boldsymbol{p}$. In these validation exercises $N = 100$ measurements of indenter penetration are considered at 25 equal interval stages of both loading and unloading branches of the indentation curves generated by the two tests. The discrepancy function ω, Eq. (8), is here the Euclidean norm of the difference between the two vectors. No computational changes would be implied by the formulation of function ω as a quadratic form of such a difference centered on the inverse of the covariance matrix of the expected measurement errors, if available in practical applications. To the present purposes the covariance matrix is assumed as unit matrix, consistently with Eq. (8).

The minimization of the discrepancy function is performed here by a "Trust Region Algorithm" (TRA), using its implementation in Matlab, see [20]. Details of TRA are available in a vast literature on mathematical programming procedure, e.g. [21]. Only the following main peculiar features are here reminded: for initialization a parameter vector $\mathbf{p}$ is chosen within the "search domain" in the space of the sought parameters; at the beginning of each iteration step first-order derivatives of $\omega(\mathbf{p})$ are approximated by finite differences and employed to generate approximations of gradient $\mathbf{g}$ and jacobian $\mathbf{J}$ of ω; with Hessian approximation by means of $\mathbf{g}$ and $\mathbf{J}$ a quadratic programming problem is solved in the parameters increments $\boldsymbol{\Delta p}$ as linear combination of $\mathbf{g}$ and $\mathbf{J}$ under constraints which include "trust region" bounds; solution $\hat{\mathbf{p}}$ is reached at ω minimum according to a preselected convergence criterion. As remedies for possible lack of convexity of $\omega(\mathbf{p})$ and possible consequent local minimum, the TRA can be applied again with other initializations.

In pseudo-experimental exercises the absolute minimum might be checked by assessment of compatibility of $\omega(\hat{\boldsymbol{p}})$ with round-off errors accumulation along TRA applied to computed pseudo-experimental data.

In Figs. 6 and 7 the convergence of TRA applied to the present example is visualized starting from two quite different initializations. In both numerical exercises after 14 and 16 iterations all the 4 variable parameters exhibit an "error" less than 0.5 %, as difference from their values employed in the test simulation which had generated the pseudo-experimental data employed in the two inverse analyses.

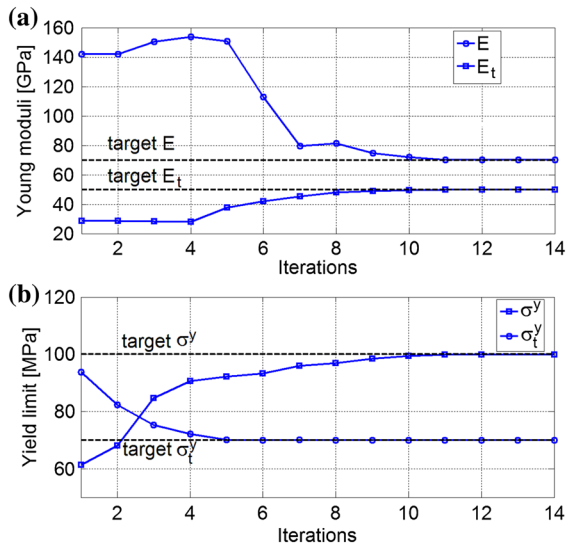

Fig. 6 Convergence of TRA minimization of discrepancy function ω from initialization 1: **a** elastic parameters and **b** plastic parameters

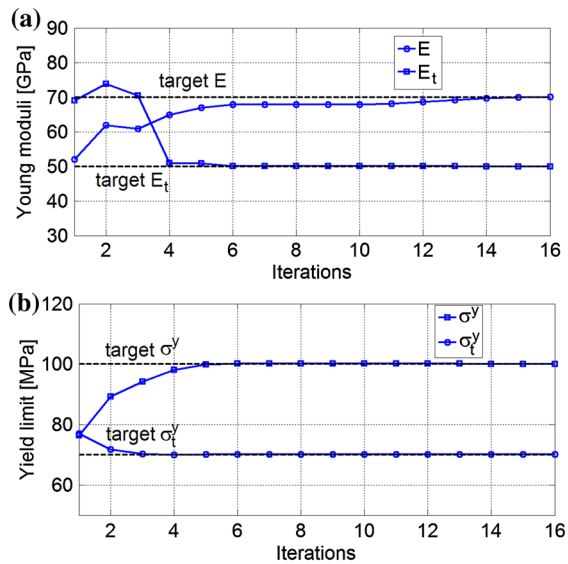

Fig. 7 Same as in Fig. 6, starting from different initializations

Clearly, the TRA iteration sequence for the discrepancy minimization requires a large number of direct analyses for the computation of (first order) finite differences of function $\omega(\mathbf{p})$ at each step. Specifically, all together in each one of the above numerical examples, computing time for one identification have been approximately 80 h of CPU time by a computer with processor i5 and 6 GB of RAM memory.

Table 2 Lower and upper bounds which define the "search domain" in the space of the parameters [MPa]

	E	E_t	σ^Y	σ_t^Y
Lower bounds	40,000	40,000	50	50
Upper bounds	120,000	120,000	150	150

Even longer computing times would probably be necessary by other algorithms (such as Genetic Algorithms) apt to reach the absolute minimum of the discrepancy function $\omega(\boldsymbol{p})$. Therefore recourse to a "model reduction" procedure as outlined in what follows provides meaningful practical advantages in industrial applications of the above inverse analysis.

5.2 Proper orthogonal decomposition for economical inverse analysis

The model reduction procedure adopted herein is a "proper orthogonal decomposition" (POD) followed by interpolations through "radial basis functions" (RBF). Mathematical and computational details are available in, e.g., [21, 23, 24] and will not be considered here. Only an operative outline, with some numerical features and results, is provided in what follows.

(α) In the four-dimensional space of the sought parameters the "search domain" is defined through the lower and upper bounds suggested for each parameter by a hypothetical "expert" in the specific engineering area (see, Table 2). Here the interval center coincides with the "reference value" of the parameters (specified in Sect. 3) and each interval is subdivided in 3 equal subintervals. Such subdivision is exploited to generate a regular grid of $M = 4^4 = 256$ "nodes". Alternative approaches based on randomness, might be considered in other applications.

(β) By conferring to the $P = 4$ material parameters the values which are the coordinates of each one of the grid nodes selected in (α), the two tests are simulated by the chosen FE code M times. This is a heavy computational burden, as already mentioned: in the present example about 350 h by a computer with processor i5 and 6 GB of RAM memory.

(γ) The vectors $\mathbf{u}_i$, i = 1…M, (called "snapshots" in the relevant literature) are gathered in a matrix $\mathbf{U}$ of order N × M (here 100 × 256), which is employed to generate the (symmetric, positive semidefinite, of order M and rank N) matrix $\mathbf{D} = \mathbf{U}^{\mathrm{T}} \cdot \mathbf{U}$. Eigenvectors and eigenvalues of matrix $\mathbf{D}$ are computed, and eigenvectors corresponding to the smaller eigenvalues (i.e. those smaller by 5 orders of magnitude and more with respect to the largest one) are neglected so that only $\hat{N}$ are preserved (here $\hat{N} = 5$). After this "truncation" a matrix $\hat{\Phi}$ of order $\hat{N}\,x\,N$ is computed such that:

$$\mathbf{u}_i \cong \hat{\mathbf{u}}_i = \hat{\Phi} \cdot a_i, \quad i = 1 \ldots M \tag{9}$$

The matrix $\hat{\Phi}$ (usually called "reduced optimal reference basis") generates snapshots approximations governed by "amplitude" vectors $\mathbf{a}_i$ with dimension $\hat{N}$, computed by the following equation:

$$\mathbf{A} \equiv [\,\mathbf{a}_1 \quad \ldots \quad \mathbf{a}_M\,] = \hat{\Phi} \cdot \mathbf{U} \tag{10}$$

Intuitive motivation and mathematical proofs of the above computational development can at present be found e.g. in [22, 23].

(δ) Now let $\mathbf{p}$ be a parameter vector (within the search domain) at a stage of the TRA applied to the minimization of the discrepancy function $\omega(\mathbf{p})$. Instead of simulating the test by FE, the corresponding "snapshots" $\mathbf{u}(\mathbf{p})$ can be assessed by the reduced basis $\hat{\Phi}$ when the amplitude vector $\mathbf{a}_i$ is known. In order to compute $\mathbf{a}_i$, "radial basis functions" (RBF) g_i are considered here for all M (=256) nodes:

$$g_i(\mathbf{p}) = \frac{1}{\sqrt{\|\mathbf{p} - \mathbf{p}_i\| + c^2}}, \; i = 1 \ldots M \tag{11}$$

The RBF theory, including the strategy for the selection of the "coefficient" c (here $c = 1$), is available e.g. in [28]. A component a^k ($k = 1 \ldots M$) of the amplitude vector as function of variable vector $\mathbf{p}$ is expressed as linear combination of the RBFs, Eq. (11), and the coefficients b_j^k, with $j = 1,\ldots, M$, are computed by imposing, when $\mathbf{p}$ coincides with a grid node $\mathbf{p}_i$, that the dependent variable a^k coincides with the corresponding component of the amplitude $a_k(\mathbf{p}_i)$ provided by Eq. (10).

Therefore, the computations to perform are reduced to the solution of a system of linear algebraic equations with the coefficients b_j^k, $j = 1,\ldots,M$ and $k = 1, \ldots, \hat{N}$ as unknowns gathered in matrix $\mathbf{B}$, namely:

$$\mathbf{A} = \mathbf{B} \cdot \mathbf{G} \text{ with } \mathbf{B} = \left[b_j^k\right] \tag{12}$$

where the known matrix $\mathbf{A}$ is computed by Eq. (10), while the known matrix $\mathbf{G}$ collects the values of

adopted RBF (Eq. 11), computed in all M "nodes", namely:

$$\mathbf{G} = \left[g_i(\mathbf{p}_j)\right] \tag{13}$$

(ε) When the coefficients b_j^k have been computed, once for all, as solution of Eq. (12), for any new parameter vector **p**, generally different from the M grid nodes, the components of the corresponding "reduced amplitude" vector **a** are provided by interpolation through RBF, namely:

$$a^k(\mathbf{p}) = \sum_{j=1}^{M} b_j^k \cdot g_j(\mathbf{p}),\ k = 1,\ldots\hat{N} \tag{14}$$

Through the reduced basis $\hat{\Phi}$ the resulting amplitude vector **a** leads to the "snapshot" **u**, namely:

$$\mathbf{u}(p) = \hat{\Phi} \cdot \mathbf{a}(\mathbf{p}) \tag{15}$$

Equations (14) and (15) replace further test simulation by FE, since they generate, for any vector of sought parameters within the search domain, an approximation of the vector of the measurable quantities. Of course, the accuracy of such approximation depends, in an easily controllable way, on the "truncation" in terms of eigenvalues of matrix **D**, and on the above RBF interpolations.

(η) Finally, numerical comparisons should be performed between discrepancy minimization by an algorithm like TRA with repeated FE simulations of the test and by the same algorithm fed by the above described POD-RBF procedure, stages (α) to (ε). Such comparison, exemplified in what follows, should concern both the further approximations implied by POD and the advantages of POD in terms of computing efforts for the parameter estimation.

5.3 Numerical checks on estimation stability and accuracy

A usual procedure is here applied first in order to assess the preceding inverse analysis as for its computational "stability", namely as for the transition from experimental errors on the consequent errors of the parameters estimates.

The pseudoexperimental data provided by direct analysis in Sect. 5.1 are supposed to be affected by random perturbation with uniform probability densities first between ±1 %, and then between ±2 and ±3 %. In Table 3a, the consequences of such "noises" in the input of 10 inverse analyses according to POD + TRA procedures (see, Sect. 5.2) are quantified, in terms of percentage mean value and Gaussian standard deviation, on the output of estimate sets.

Table 3 Consequences (in percentage) on parameter estimates caused by perturbation of the measurements on indentation curves: (a) average and standard deviations due to random experimental noises in percentage (based on 10 random noise extractions); (b) estimation changes due to additive errors in experimental data on penetration depth

	Noise ± 1 %	Noise ± 3 %	Noise ± 5 %
(a)			
E	1.42 ± 3.77	3.02 ± 3.77	5.08 ± 4.22
E_t	1.33 ± 0.75	3.29 ± 3.05	5.56 ± 4.55
σ^Y	0.53 ± 0.33	1.23 ± 0.93	2.19 ± 1.32
σ_t^Y	0.67 ± 0.31	1.21 ± 1.01	2.71 ± 1.36
	Error + 1 μm	Error + 3 μm	Error + 5 μm
(b)			
E	1.03	4.27	9.44
E_t	1.92	5.14	11.43
σ^Y	0.21	0.65	1.29
σ_t^Y	0.52	0.72	1.32

Another computational check led to results in Table 2b: data on indenter penetration depth are increased by 1, 3 and 5 microns as measurement errors and employed as inverse analysis inputs; the consequences on the outputs are gathered in percentages.

The conclusions of the above and similar other numerical exercises are as follows: (i) in the parameter identification context investigated herein, the resulting estimates are reachable by a fashionable economical POD + TRA computational procedure as for the four main parameters through double indentations by means of ellipsoidal indenters; (ii) anisotropic, transversally isotropic plasticity parameters turn out to be more accurately identifiable than Young's moduli.

6 On "a priori" assumptions of constitutive parameters

6.1 Calibration of transversally anisotropic models

An increase in the number of constitutive parameters to identify implies exponential growth of computing

efforts and also may imply ill-posedness of the inverse analysis problem, if the number of available data does not increase. In the present study on potentialities and limits of a novel procedure for anisotropic material characterization by indentation alone, these issues are particularly meaningful. In the preceding Sections isotropy had been assumed in the transversal plane orthogonal to the indented surface and to the principal direction (axis x_1) supposed "a priori" known. Such restrictive hypothesis may be hardly acceptable in several practical situations, e.g. in applications to laminated products. An improvement to the assumptions on the material model to calibrate is here investigated, namely two Young's moduli E_2 and E_3 (instead of E_t) and two yield stresses σ_2^Y and σ_3^Y (instead of σ_t^Y) are now the parameters to identify by the double indentation test considered so far, but no longer with transversal isotropy assumption in the plane orthogonal to the principal axis x_1.

The results of these computations are as follows: (i) the convergence of TRA visualized in Fig. 8 (with parameters normalized by the relevant reference values) suggests that the inverse problem is still well-posed, despite the increase (from 4 to 6) of the parameters number estimated now on the basis of unaltered pseudo-experimental data and starting from similar initializations; (ii) the following differences emerge between the resulting estimates and the relevant reference values attributed to the sought parameters for direct analysis generating the pseudo-experimental data: $\Delta E_1 = -0.5$ %, $\Delta E_2 = 0.73$ %, $\Delta E_3 = -4.6$ %, $\Delta\sigma_1^Y = 0.41$ %, $\Delta\sigma_2^Y = -0.65$ % and $\Delta\sigma_3^Y = -2.71$ %. (iii) the growth of computing time as consequence of the transition from 4 to 6 estimations amounts to about 40 %.

6.2 On consequences of possible erroneous transversal isotropy assumption

In view of remarkable computing efforts growth due to increases in the number of parameters to estimate, desirable are provisions apt to provide possible remedies in practical applications. Transversal isotropy hypothesis assumed in Sect. 5 might be adopted in practice as simplification even if it is not corroborated by expertise and hence might be erroneous. On this issue the following computations may lead to some orientative conclusions useful for practical applications.

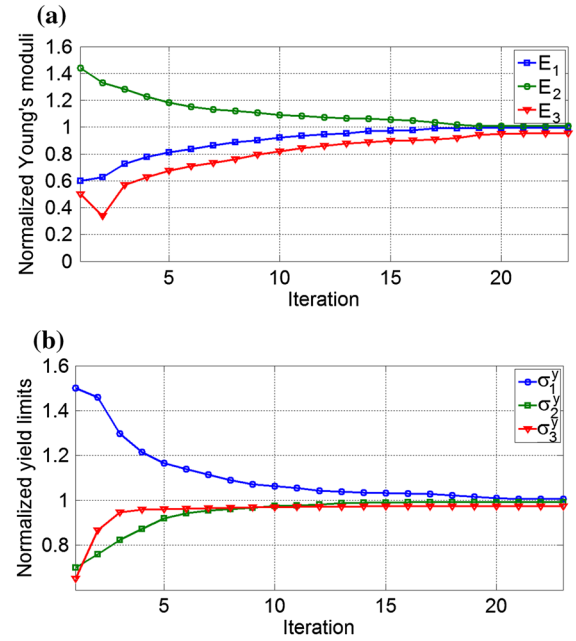

Fig. 8 Convergence of TRA with 6 parameters to identify (no transversal isotropy) on the basis of the same pseudo-experimental data as for convergence plots in Figs. 6 and 7: **a** Young moduli; **b** yield stresses

(a) First transversal anisotropy is generated in material model by attributing Young's modulus E_3 and yield stress $\bar{\sigma}_3^Y$ in the direction of the indenter axis x_3 values increased by 20 % with respect to the values considered in what precedes, whereas all other parameters are preserved unaltered. A direct analysis, as usual, provides new pseudo-experimental data which obviously reflect the transversal anisotropy. The inverse analysis starting from such data is performed again by the TRA procedure but based on transversal isotropy hypothesis like in Sect. 5. This inverse analysis leads to 4 estimates obviously affected by errors. Such errors consisting of the differences between the estimates (only 4 due to assumed isotropy) and the "true" parameters are gathered in Table 4a.

(b) The above numerical exercise is repeated starting from 20 % increments attributed now to elastic modulus E_t^2 and yield limit $\bar{\sigma}_2^Y$ along the axis x_2 in the indented surface and orthogonal to principal direction x_1. The results are presented in Table 4b.

Table 4 Comparisons between actual parameters with transversal anisotropy ("target values") and their estimates with the assumption of transversal isotropy

Parameter	Target value	Estimated value
(a)		
$\bar{E}$	70 GPa	72.5 GPa
$\bar{E}_2$	50 GPa	51.9 GPa
$\bar{E}_3$	60 GPa	
$\bar{\sigma}^Y$	100 MPa	101.8 MPa
$\bar{\sigma}_2^Y$	70 MPa	70.9 MPa
$\bar{\sigma}_3^Y$	84 MPa	
(b)		
$\bar{E}$	70 GPa	66.7 GPa
$\bar{E}_2$	60 GPa	56.8 GPa
$\bar{E}_3$	50 GPa	
$\bar{\sigma}^Y$	100 MPa	98.0 MPa
$\bar{\sigma}_2^Y$	84 MPa	82.2 MPa
$\bar{\sigma}_3^Y$	70 MPa	

The above computations (and others not presented here for brevity) lead to the following, merely orientative remarks: the simplifying hypothesis of transversal isotropy may be acceptable in industrial environments dealing with products expected to be moderately anisotropic in the plane orthogonal to the principal direction of general anisotropy generated by a routine production process.

7 Closing remarks

Indentation tests are at present more and more frequently employed in a growing number of industrial contexts and at various scales because of remarkable advantages (un-destructivity, rapidity, economy) with respect to traditional experiments for mechanical characterization of materials. In this paper the parameter calibration based only on instrumented indentations has been studied with reference to a popular simple orthotropic elastic plastic constitutive model concerning laminated structural metals. First, orthotropy has been assumed with known principal directions on the specimen and with isotropy in the plane orthogonal to the indented surface. Under such assumption, the anisotropic Hill model of perfect plasticity has been adopted and the parameters considered for estimation have been two elastic Young's moduli and two yield limits. Subsequently, the restriction of isotropy in the "transversal plane" has been removed and 6 parameters (3 Young's moduli and 3 yield limits) have been considered for the identification procedure.

Elastic moduli can be identified at present by fully non-destructive test like resonance, clearly unable to estimate inelastic parameters. Advantages of the employment of a single experimental equipment, like the present instrumented indenter, arise in most industrial environments active in structural diagnoses.

The main features and conclusions of the preliminary study outlined in this paper, can be synthesizes as follows.

(a) Two indentation tests in near locations by an indenter with elliptical cross-section, turned 90 degrees, can provide experimental data consisting of indentation curves only, but sufficient for the estimation of the main parameters governing the anisotropy at least in simple elastic–plastic models without hardening.
(b) The transition from traditional conical or spherical shape governed by one parameter (angle or diameter respectively) to new shapes with elliptical cross-sections is governed by another parameter (here "ellipticity" α). Both parameters, particularly α, can be optimized merely by test simulations in order to ensure "sensitivity" in the sense of remarkable difference between the curves generated by the two indentations.
(c) The practical advantages provided by the employment of an indenter alone for generation of data sufficient for model calibration (no data on imprint geometry) are here additional to the practical advantages of preliminary proper orthogonal decomposition and of fast in situ estimation of material parameters.

After this preliminary study, research in progress concerns extensions of the present approach to estimation of more parameters (hardening, viscosity) or/and of parameters in anisotropy with principal directions not "a priori" known.

Acknowledgments Thanks are expressed by the authors to Tetrapak Company, Modena Factory, for support to Dr. V. Buljak during his research activity in Milan.

References

1. Tabor D (1951) The hardness of metals. Clarendon Press, Oxford
2. Mott BW (1957) Microindentation hardness testing. Butterworths, London
3. Bolzon G, Maier G, Panico M (2004) Material model calibration by indentation, imprint mapping and inverse analysis. Int J Solids Struct 41:2957–2975
4. Bocciarelli M, Bolzon G, Maier G (2005) Parameter identification in anisotropic elastoplasticity by indentation and imprint mapping. Mech Mater 37:855–868
5. Vlassak J, Nix WD (1994) Measuring the elastic properties of anisotropic materials by means of indentation experiments. J Mech Phys Solids 42:1223–1245
6. Jorgensen O, Giannakopoulos AE, Suresh S (1998) Spherical indentation of composite laminates with controlled gradients in elastic anisotropy. Int J Solids Struct 58:505–513
7. Swadener JG, Pharr GM (2001) Indentation of elastically anisotropic half-spaces by cones and parabolas of revolution. Philos Mag A 81:447–466
8. Vlassak J, Ciavarella M, Barber JR, Wang X (2003) The indentation modulus of elastically anisotropic materials for indenter of arbitrary shape. J Mech Phys Solids 51:1701–1721
9. Swadener JG, Rho J-Y, Pharr GM (2001) Effect of anisotropy on elastic moduli measured by nanoindentation in human tibial cortical bone. J Biomed Mater Res 57:108–112
10. Hengberger S, Enstoem J, Peyrin F, Zysset P (2003) How is the indentation modulus of bone related to its macroscopic elastic response? A validation study. J Biomech 36:1503–1509
11. Yonezu A, Kuwahara Y, Yoneda K, Hirakata H, Minoshima K (2009) Estimation of anisotropic plastic properties using single spherical indentation-an FEM study. Comput Mater Sci 47:611–619
12. Yonezu A, Tanaka M, Kusano R, Chen X (2013) Probing out-of-plane anisotropic plasticity using spherical indentation: a numerical approach. Comput Mater Sci 79:336–344
13. Nakamura T, Gu Y (2007) Identification of elastic-plastic anisotropic parameters using instrumented indentation and inverse analysis. Mech Mater 39:340–356
14. Bocciarelli M, Maier G (2007) Indentation and imprint mapping method for identification of residual stresses. Comput Mater Sci 39:381–392
15. Buljak V, Maier G (2012) Identification of residual stresses by instrumented elliptical indentation and inverse analysis. Mech Res Commun 41:21–29
16. Hill R (1948) A theory of yielding and plastic flow of anisotropic metals. Proc R Soc Lond A 193:281–297
17. Lubliner J (2008) Plasticity theory. Dover Publications, New York
18. Jirasek M, Bazant Z (2002) Inelastic Analysis of Structures. Wiley, London
19. Abaqus (2006) Standard, Theory and User's manuals, Release 6.7, Simulia Inc., Providence, RI 02909, USA
20. Matlab (2002) User's guide and optimization toolbox, release 6.13, The Math Works Inc., USA
21. Nocedal J, Wright SJ (2006) Numerical optimization. Springer, New York
22. Buljak V (2012) Inverse analysis with model reduction – Proper Orthogonal Decomposition in structural mechanics. Springer, Berlin
23. Jolliffe IT (1986) Principal component analysis. Springer, New York
24. Buljak V, Maier G (2011) Proper orthogonal decomposition and radial basis functions in material characterization based on instrumented indentation. Eng Struct 33:492–501
25. Kleiber M, Antunez H, Hien TD, Kowalczyk P (1997) Parameter sensitivity in non-linear mechanics. Willey, Chichester
26. Bui HD (1994) Inverse problems in the mechanics of materials: an introduction. CRC Press, Boca Raton
27. Tarantola A (2005) Inverse problem theory and methods for model parameter estimation. Society for industrial and Applied Mathematics, Philadelphia
28. Buhmann MD (2003) Radial basis functions. Cambridge University Press, Cambridge